NATIONAL ADVISORY COMMITTEE FOR AERONAUTICS

RESEARCH MEMORANDUM

TRANSONIC FLUTTER INVESTIGATION OF MODELS OF THE ALL-MOVABLE HORIZONTAL TAIL OF A FIGHTER AIRPLANE

By Thomas B. Sellers

SUMMARY

A transonic flutter investigation of models of the all-movable horizontal tail of a fighter airplane has been conducted in the Langley transonic blowdown tunnel. The models were dynamically and elastically scaled by criteria which provide a flutter safety margin. The results showed that the model had a stiffness margin which was insufficient to provide adequate safety from flutter at a Mach number of 1.06. An increase in the model pitch stiffness of approximately 40 percent of the anticipated design value resulted in an adequate margin. With the model pitch axis moved forward from 77 percent to 58 percent of the root chord, 83 percent of the anticipated design pitch stiffness was necessary to provide an adequate margin at sea level.

INTRODUCTION

A flutter investigation of models of the all-movable horizontal tail of a new fighter airplane has been made in the Langley transonic blowdown tunnel. The panels of the models were dynamically and elastically scaled. The tail pitch and fuselage vertical bending degrees of freedom were also simulated. The primary purpose of the investigation was to determine if the model would be flutter-free in simulated sea-level flight at Mach numbers from 0.8 to 1.3. Additional tests were made to study the effect of varying the pitch stiffness and pitch-axis location.

SYMBOLS

b	half-chord parallel to plane of symmetry, ft
b_s	half-chord parallel to plane of symmetry at intersection of tail panel and fuselage, ft
c	root chord at plane of symmetry, ft
f	flutter frequency, cps
f_i	measured natural frequencies ($i = 1, 2, 3, \ldots$), cps
EI	panel bending stiffness, lb-ft^2
GJ	panel torsional stiffness, lb-ft^2
I_α	mass moment of inertia about an axis passing through center of gravity and perpendicular to plane of symmetry per unit length of exposed panel span, slug-ft^2/ft
M	Mach number
m	mass of panel per unit length of exposed panel span, slugs/ft
l	length scale factor, typical length of model divided by corresponding length of airplane
m'	mass scale factor, typical model mass divided by corresponding airplane mass
q	dynamic pressure, lb/sq ft
t	time scale factor, time required for tunnel airstream to move 1 model chord length divided by time required for airplane to move 1 airplane chord length
T	static temperature, $^\circ R$
V	free-stream velocity, ft/sec
$\bar{V}$	reduced velocity based on representative natural frequency, $\frac{V}{bf_i}$

[redacted]

x_{cg} distance in semichords (measured parallel to plane of symmetry) from midchord to center-of-gravity position measured positive rearward from midchord

η nondimensional coordinate along exposed panel span, fraction of exposed panel span

η_{cg} value of η at center of gravity of strip

ρ air density, slugs/cu ft

μ ratio of mass of air contained in a frustum of a cone with base diameter equal to streamwise root chord and top diameter equal to streamwise tip chord

Subscripts:

M model

A airplane

MODELS

Model Plan Form

The plan form and overall dimensions of the horizontal-tail models are shown in figure 1. The plan form was a modified delta with slightly rounded tips. The model tested was 1/13.1 of the full-scale tail dimensions and had the leading and trailing edges swept back 55° and 15°, respectively. The tail had an aspect ratio of 3.45 and NACA 65A003 modified airfoil sections parallel to the plane of symmetry.

Scaling

In scaling the airplane properties, it was required that the nondimensional mass and stiffness distributions should be the same for the model as for the airplane. The mass and stiffness levels for the model were obtained by specifying the scale factors for the fundamental quantities involved: length, mass, and time.

The size of the model was limited by the tunnel-wall interference effects, and on the basis of past experience the length scale factor was chosen to be

$$l = 0.076 \qquad (1)$$

[redacted]

The mass scale factor was obtained from a requirement that the mass ratio μ should be the same for the model as for the airplane, which results in

$$m' = \frac{\rho_M}{\rho_A} l^3 \tag{2}$$

In order to locate simulated sea-level altitude in the tests near the middle of the tunnel density range available at a Mach number of 1, the density ratio was chosen to be $\rho_M/\rho_A = 2.00$. This location of simulated sea-level altitude allows altitudes below sea level to be obtained and makes it possible to indicate flutter margins for cases wherein flutter does not occur above sea level.

The time scale factor was obtained from a requirement that the reduced velocity $\overline{V}$ should be the same for the model as for the airplane, which results in

$$t = \left(\frac{V_M}{V_A}\right)^{-1} l$$

Since the Mach number is the same for the model as for the airplane, the time scale factor may be written

$$t = \left(\frac{T_M}{T_A}\right)^{-1/2} l \tag{3}$$

The static temperature for the airplane T_A is a function only of altitude and for sea-level altitude was taken to be 519° R. However, in the tunnel, the temperature continually drops as air is expended from the reservoir so that the temperatures obtained at the various flutter points during an investigation are different. A study of previous flutter data indicated that 408° R was near the average value of the static temperature that would be expected during the present runs, and this value was used to obtain the temperature ratio used in the scaling: $T_M/T_A = 0.786$.

A list of pertinent wing and flow quantities and the design scale factors used are given in table I. A factor of 0.76, which is used in some of the scaled quantities in table I, occurs because the stiffnesses of the model were made 76 percent of those which would result from application of the scale factors as specified (eqs. (1) to (3)). The

[redacted]

purpose of reducing the model stiffnesses was to provide a margin of safety in the application of the model flutter-test results to the airplane. It may be noted that the stiffness reduction results in a design reduced velocity for the model being equal, not to that of the airplane, but to that of an airplane having stiffnesses 76 percent of those of the actual airplane.

Because the temperature during a run is not a controllable quantity, the exact value of the design reduced velocity $\bar{V}$ (through eq. (3)) is not obtained. The two quantities which are controllable during a test are dynamic pressure and Mach number. If the dynamic pressure and Mach number are considered to be held constant, a change in temperature results in a change in density and velocity. Thus, the consequence of a temperature during a run different from the design temperature is that neither the reduced velocity nor the mass ratio is simulated exactly. However, a combination of reduced velocity and mass ratio, which can be expressed in terms of the dynamic pressure

$$\frac{\bar{V}_M^2}{\mu_M} \propto q_M$$

is independent of the temperature, and this combination is exactly simulated in the tests by the expedient of interpreting the simulated altitude in terms of dynamic pressure. Thus, the scale factor in table I for dynamic pressure is used to convert the dynamic pressure for the airplane at any altitude and Mach number to the dynamic pressure for the model at the same altitude and Mach number. The dynamic pressure for the airplane is assumed to be that obtained from the ICAO standard atmosphere (ref. 1). It may be noted that, for a given altitude, q/M^2 is a constant quantity.

The effect of not individually satisfying exactly the mass ratio and reduced velocity is believed to be negligible in the present investigation. Experience with a wide variety of flutter models has indicated that, at least within the operational limits of the tunnel, flutter at a given Mach number tends to occur at a constant value of dynamic pressure regardless of the individual values of density and velocity.

Model Construction

Two models were used in this investigation and are designated as models 1 and 3. A typical model, which is shown partially and completely assembled in figures 2 and 3, respectively, consisted of dynamically and elastically scaled tail panels joined together by an elastically

[redacted]

scaled crossover yoke, an elastically scaled flexibility fixture, and a mounting block with cover. The details of the tail-panel construction are shown in the photograph of figure 4. The panels were made with a tapered hollow aluminum-alloy box spar, the center line of which was located along the 0.57 local chord line and extended from the panel root to the tips. Several aluminum-alloy ribs, which were channel shaped in cross section, were welded to the spar. Mahogany strips formed the leading and trailing edges and completed the panel framework. The framework was filled with balsa and the entire structure was covered with silk.

The U-shaped crossover yoke was rectangular in cross section and was made of aluminum alloy. A 0.088-pound lead weight (fig. 2) was attached to the upstream vertical face of the crossover yoke in order to locate the center of gravity of the tail structure at the correct position. This weight was interchangeable and was mounted on each model prior to testing.

The flexibility fixture is shown in figure 5 as assembled for the rear pitch-axis location. The model was attached to the two tail mounting pads (one on each side) with two screws in each pad. Flexure hinges at the rear of each pad fixed the location of the pitch axis. The pitch-spring links indicated in figure 5 were small bolts. These bolts connected the front end of the mounting pads with the pitch springs. The pitch springs and the fixed part of the flexure pivots were attached to the main part of the flexibility fixture by two screws passing through each of the two rearward mounting lugs (fig. 5). The fuselage vertical bending was simulated by the fuselage vertical spring shown at the front of the fixture.

The location of the pitch axis was changed from the rearward locations (figs. 1 and 5) to the forward location by removing as a unit the flexure pivot assembly, tail mounting pad, pitch-spring link, and pitch spring, then rotating this unit 180°, and attaching the fixed portion of the flexure pivot and the fixed end of the pitch spring to the forward mounting lug (fig. 5). The forward and rearward pitch axes were located at the 0.58c and 0.77c stations, respectively. The pitch stiffness was varied by inserting pitch springs of varying thicknesses.

Physical Properties of Models

The values of torsional, bending, and pitch stiffness of a typical model were determined by the method described in reference 2. Briefly, the system was an optical one through which the deflections of the tail panels were magnified and measured when a known moment was applied to the panel. In order to determine the panel mass and center-of-gravity

[redacted]

location, a panel was cut into several chordwise segments (parallel to the plane of symmetry) approximately 1/2 inch wide. Each segment was weighed and its center of gravity located. The moment of inertia of each segment about an axis passing through the center of gravity of the segment and perpendicular to the plane of symmetry was found by swinging each segment on a torsional pendulum.

The center-of-gravity location, mass moment of inertia, mass per unit length, and local chord ratio for several spanwise stations are tabulated in table II. The values of EI and GJ for the two models are plotted in figure 6. The mass-property differences between the tail panels were assumed to be small, and only one set of mass properties are given.

The moment of inertia about the forward and rearward pitch axes of the tail panel assemblies which included the tail panels and crossover yoke with lead weight was determined by swinging the tail panel assembly as a physical pendulum. The values of moments of inertia obtained in this manner were 0.002195 and 0.001947 slug-ft^2 for the forward and rearward hinge-line locations, respectively. The mass of the tail structure was 0.0157 slug and the center of gravity was located at the 0.65c station and 0.21 inch below the tail-panel chord plane.

The frequencies that correspond to the natural modes of vibration were determined by exciting the tail panels over a range of frequencies with an electromagnetic vibrator. Node lines were defined by sprinkling salt onto the wing while the panel was excited at a natural frequency, and the stationary grains of salt formed along the panel node line. The modes of vibration for the model with fuselage flexibility included yawing modes which tended to destroy the node lines indicated by the grains of salt and which made the selection of the natural frequencies, node lines, and modes quite difficult. In order to obtain a better indication of the natural frequencies, the output of the strain gage that responded to the particular mode of interest together with the input to the vibrator were fed into the vertical and horizontal axes of an oscilloscope. When a natural frequency was reached, the trace on the oscilloscope would form an elliptical pattern which was symmetrical about the horizontal and vertical axes. Also, the model was viewed under a stroboscopic light which helped to identify the mode of vibrations. The cantilevered modes were obtained with the tail panels clamped just inboard of the fuselage line. The natural frequencies and corresponding node lines for the models cantilevered and with fuselage freedoms are presented in figures 8 and 9, respectively.

[redacted]

APPARATUS AND TESTS

Tunnel and Model Support System

The flutter tests were conducted in the Langley transonic blowdown tunnel which is a 26-inch octagonal slotted tunnel. The tunnel operates over a range of Mach numbers from approximately 0.6 to 1.4. The operating characteristics (tunnel dynamic pressure may be increased at a constant Mach number) are particularly suitable for flutter testing and these characteristics are discussed in detail in reference 2. Because of the expansion of air in the reservoir during a run, the stagnation temperature continually decreases; thus, the test-section velocity is not uniquely defined by the Mach number.

A schematic drawing of the model support system is shown in figure 7. The mounting block was rigidly mounted in a 3-inch-diameter cylindrical sting fuselage. The sting fuselage extended upstream into the subsonic flow region of the tunnel entrance cone, and the downstream end was supported by a strut which spanned the tunnel. The extension of the sting into the subsonic region of the tunnel prevents the formation of a bow wave and its possible reflection on the model. A discussion of the effects on flutter tests of the degree of root fixity afforded by the support system and the sting boundary layer is presented in reference 3.

Instrumentation

Tunnel stagnation pressure, static pressure, and stagnation temperature were transmitted by suitable pickups to amplifying equipment and recorded on a multichannel automatic recording oscillograph simultaneously with the strain-gage outputs from the model. Each tail panel was equipped with two sets of strain gages which responded to panel bending and torsional deflections. Pitch deflections were detected by a set of strain gages mounted on weak auxiliary springs (removed for clarity in figs. 2 to 5) which were connected between the free end of the pitch spring and the forward or rearward mounting lugs on the fuselage flexibility fixture. Two auxiliary springs were used, one for each pitch spring. The fuselage vertical deflections were detected by a set of strain gages which were mounted on the fuselage vertical spring.

A flutter-indicating system was used during the investigation to detect the onset of flutter. The system consisted of two oscilloscopes, one for each tail panel. The outputs from the bending and torsion gages for each panel were fed into the horizontal and vertical axes, respectively, of an oscilloscope. Before the wing fluttered, the trace on

[redacted]

the oscilloscope was random but, when the bending and torsion frequencies were the same (flutter), the trace formed a simple Lissajous figure.

Flutter Tests

The flutter tests were made with the model mounted along the tunnel center line. Several low-speed runs were made and the model angle of attack was adjusted until there was no appreciable deflection of the panel tips. This angle was assumed to be the angle of zero lift.

At the beginning of a typical flutter test, the oscillograph was started and the tunnel stagnation pressure was increased until the model was seen to flutter or the Lissajous figure was obtained on either one or both of the oscilloscopes. When flutter was apparent or the scaled airplane flight boundary was reached, the tunnel speed was reduced immediately. After each run, the model was checked visually for damage. Also, the tip of the panel was deflected and released and the resulting decay of free-bending oscillations was recorded on the oscillograph. This was done in an effort to detect any structural damage suffered by the panel in the previous run. Tests were made with several values of pitch stiffness with the pitch axis at the forward and rearward locations. The infinite pitch stiffness tests were made with the fuselage flexibility fixture and pitch freedom locked by suitable shimming.

DISCUSSION OF RESULTS

General Comments

The results of the flutter tests are given in table III and plotted in figure 10 as dynamic pressure q against Mach number with curves of simulated altitude also indicated. Several data points in figure 10 are denoted as points of intermittent flutter. The term intermittent flutter describes a condition wherein, for short periods of time, the frequency of the motions for the various degrees of freedom approach a common value.

As stated in the "Scaling" section of this report, the model stiffnesses were 76 percent of the scaled airplane stiffnesses. Since to a first-degree approximation for most configurations, the dynamic pressure required for flutter varies directly with the model stiffness level, a flutter point obtained with the model at a given Mach number and dynamic pressure suggests that the airplane will flutter at the same Mach number at a simulated altitude corresponding to a dynamic pressure 32 percent

[redacted]

higher $\left(\frac{1}{0.76} = 1.32\right)$ than that obtained with the model. This statement assumes, of course, that the model exactly simulates the airplane.

Simulated Airplane Tests

Model 3 simulated the airplane design configuration (rearward pitch-axis location and pitch stiffness of 788 ft-lb/radian) and was tested at Mach numbers of 0.85 and 1.06. The data in figure 10 show intermittent flutter at $M = 0.85$ and $q = 1{,}880$ lb/sq ft, which is a value of q slightly above the simulated sea-level flight boundary. However, at $M = 1.06$ and $q = 2{,}330$ lb/sq ft destructive flutter occurred. This point was within the simulated flight boundary of the airplane, which indicates that the model had an insufficient stiffness margin.

Effects of Pitch Stiffness With Rearward Pitch Axis

In order to indicate the effect of pitching stiffness, model 1 was tested with the pitching degree of freedom locked. For these tests, the fuselage vertical bending degree of freedom was also locked. As shown in figure 10, flutter was not encountered within the flight boundary with the model cantilevered. When the pitch stiffness was decreased to 1,093 ft-lb/radian, intermittent flutter was present at the flight boundary. With this intermediate pitch stiffness, one flutter point was obtained at a Mach number of 0.8. This flutter point was considerably above the flight boundary, but it should be noted that probably a more critical Mach number would be near $M = 1.0$. In summary, with the rearward pitch axis location, increasing the pitch stiffness 40 percent of the design value allowed the model to reach the simulated flight boundary without fluttering.

Effect of Pitch-Axis Location

On the assumption that, with the pitch axis moved forward, less pitch stiffness would be required to free the model from flutter within the flight boundary, a series of tests were conducted with the pitch axis moved forward from the 0.77c station to the 0.58c station. Pitch stiffnesses of 497, 631, and 865 ft-lb/radian were tested in this phase of the investigation and the results are plotted in figure 10.

A pitch stiffness of 865 ft-lb/radian was sufficient to prevent flutter within the flight boundary. A decrease in pitch stiffness to 631 ft-lb/radian was marginal as indicated by the intermittent flutter which was obtained at the flight boundary. Further reduction in the

[redacted]

pitch stiffness to 497 ft-lb/radian resulted in intermittent flutter at $M = 0.86$, $q = 13.2$ lb/sq ft, and flutter at $M = 1.09$, $q = 18.7$ lb/sq ft, which is well within the flight boundary. Overall, the data show that with the pitch axis located at 0.58c, the pitch stiffness required to prevent flutter of the model within the flight boundary was approximately 631 ft-lb/radian or 80 percent of the design pitch stiffness of 788 ft-lb/radian.

CONCLUSIONS

An analysis of transonic flutter tests of a model of the all-movable horizontal tail of a new fighter airplane in the 26-inch Langley transonic blowdown tunnel produced the following conclusions.

1. The model with the anticipated design pitch stiffness had a stiffness margin which was insufficient to provide adequate safety from flutter at a Mach number of 1.06.

2. An increase in model pitch stiffness of approximately 40 percent of the anticipated design value resulted in an adequate margin.

3. With the model pitch axis moved forward from 77 percent to 58 percent of the root chord, 80 percent of the anticipated design pitch stiffness was sufficient to provide an adequate margin.

Langley Aeronautical Laboratory,
National Advisory Committee for Aeronautics,
Langley Field, Va., October 21, 1957.

[redacted]

REFERENCES

1. Anon.: Standard Atmosphere - Tables and Data for Altitudes to 65,800 Feet. NACA Rep. 1235, 1955. (Supersedes NACA TN 3182.)

2. Unangst, John R., and Jones, George W., Jr.: Some Effects of Sweep and Aspect Ratio on the Transonic Flutter Characteristics of a Series of Thin Cantilever Wings Having a Taper Ratio of 0.6. NACA RM L55I13a, 1956.

3. Sellers, Thomas B., and Land, Norman S.: Flutter Characteristics at Transonic Speeds of a 45° Sweptback Wing With and Without Inboard Modifications at the Leading and Trailing Edges. NACA RM L56I28, 1957.

[redacted]

TABLE I.- DESIGN SCALE FACTORS

$$\left[\frac{\rho_M}{\rho_A} = 2.00;\ \frac{T_M}{T_A} = 0.786\right]$$

Fundamental quantities:	
Length, l	0.076
Mass, $m' = \frac{\rho_M}{\rho_A} l^3$	0.877×10^{-3}
Time, $t = \left(\frac{T_M}{T_A}\right)^{-1/2} l$	0.0857
Derived quantities:	
Stream velocity, lt^{-1}	0.887
Stream dynamic pressure, $l^{-1}m't^{-2}$	1.572
Moment of inertia, l^2m'	0.0051×10^{-3}
EI and GJ, $0.76l^3m't^{-2}$	0.399×10^{-4}
Natural vibration frequencies, $\sqrt{0.76}t^{-1}$	10.17

[redacted]

TABLE II.- PHYSICAL PROPERTIES OF TYPICAL

TAIL PANEL

η_{cg}	$\frac{b}{b_s}$	x_{cg}	m, slug/ft	$I_{\alpha'}$, slug-ft^2/ft
0.038	0.953	0.093	0.0268	0.000540
.113	.878	.011	.0200	.000399
.188	.803	.086	.0106	.000148
.264	.725	-.188	.0127	.000122
.339	.659	-.091	.0152	.000197
.414	.583	-.276	.0120	.000095
.490	.510	.005	.0044	.000027
.565	.434	.051	.0084	.000041
.640	.357	.044	.0030	.000008
.716	.288	.067	.0046	.000008
.791	.210	.130	.0017	.000002
.866	.135	-.030	.0011	.000001

[redacted]

TABLE III.- TEST DATA

Test	Run	Model	Hinge-line location	Pitch stiffness, ft-lb/radian	ρ, slugs/cu ft	q, lb/sq ft	M	V, ft/sec	T, °R	f, cps	Remarks
263	1	3	Rearward	788	0.0049	1,800	0.850	856	422		Intermittent flutter
	2	↓	↓	↓	.0044	2,350	1.064	1,038	360	257	Flutter - broke
265	1	1	None	∞	.0048	1,950	.870	894	439		No flutter
	2				.0048	2,680	1.075	1,059	404		
	3				.0052	3,370	1.209	1,138	368		
	4				.0054	4,050	1.326	1,220	353		
267	1		Forward	497	.0049	1,900	.860	880	435		No flutter
	2		↓	↓	.0044	2,550	1.088	1,077	408	250	Flutter
271	1		Forward	865	.0050	1,870	.851	864	429		No flutter
	2				.0048	2,650	1.062	1,045	403		
	3				.0052	3,310	1.199	1,133	372		
	4				.0054	3,860	1.304	1,190	347		
277	1		Forward	631	.0048	1,890	.850	880	446		No flutter
	2				.0050	2,710	1.057	1,042	404		Intermittent flutter
	3				.0049	3,240	1.195	1,147	383		
	4				.0054	3,660	1.295	1,162	335		
280	1		Rearward	1,093	.0048	1,930	.868	897	444		Intermittent flutter
	2				.0047	2,680	1.079	1,068	408		
	3				.0048	2,700	1.068	1,058	409		
	4				.0050	3,230	1.190	1,137	380		
	5				.0052	3,870	1.302	1,218	364		
308	2		Rearward	1,093	.0076	2,380	.802	790	404.3	282	Flutter - broke

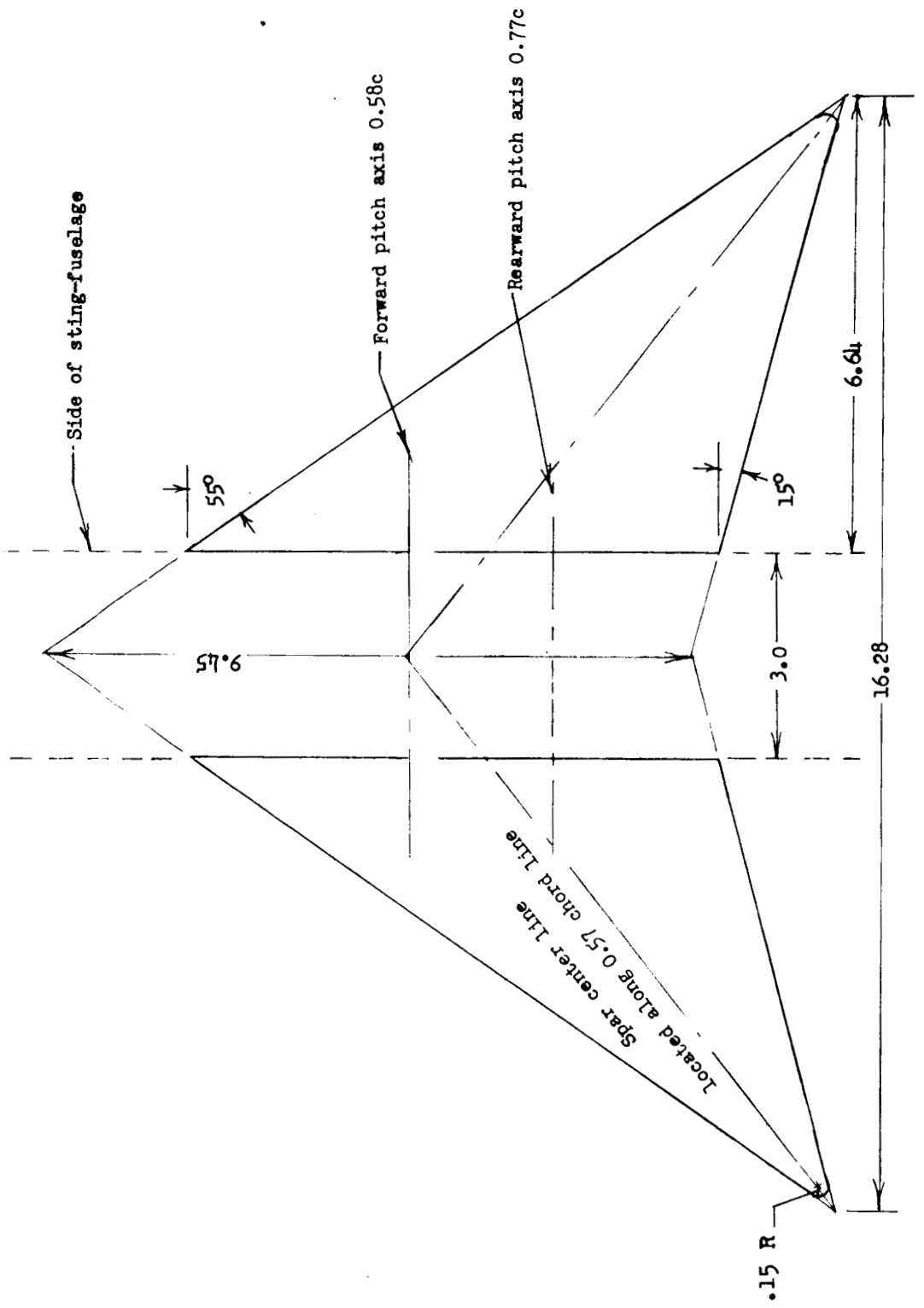

Figure 1.- Plan form of models. Dimensions are in inches.

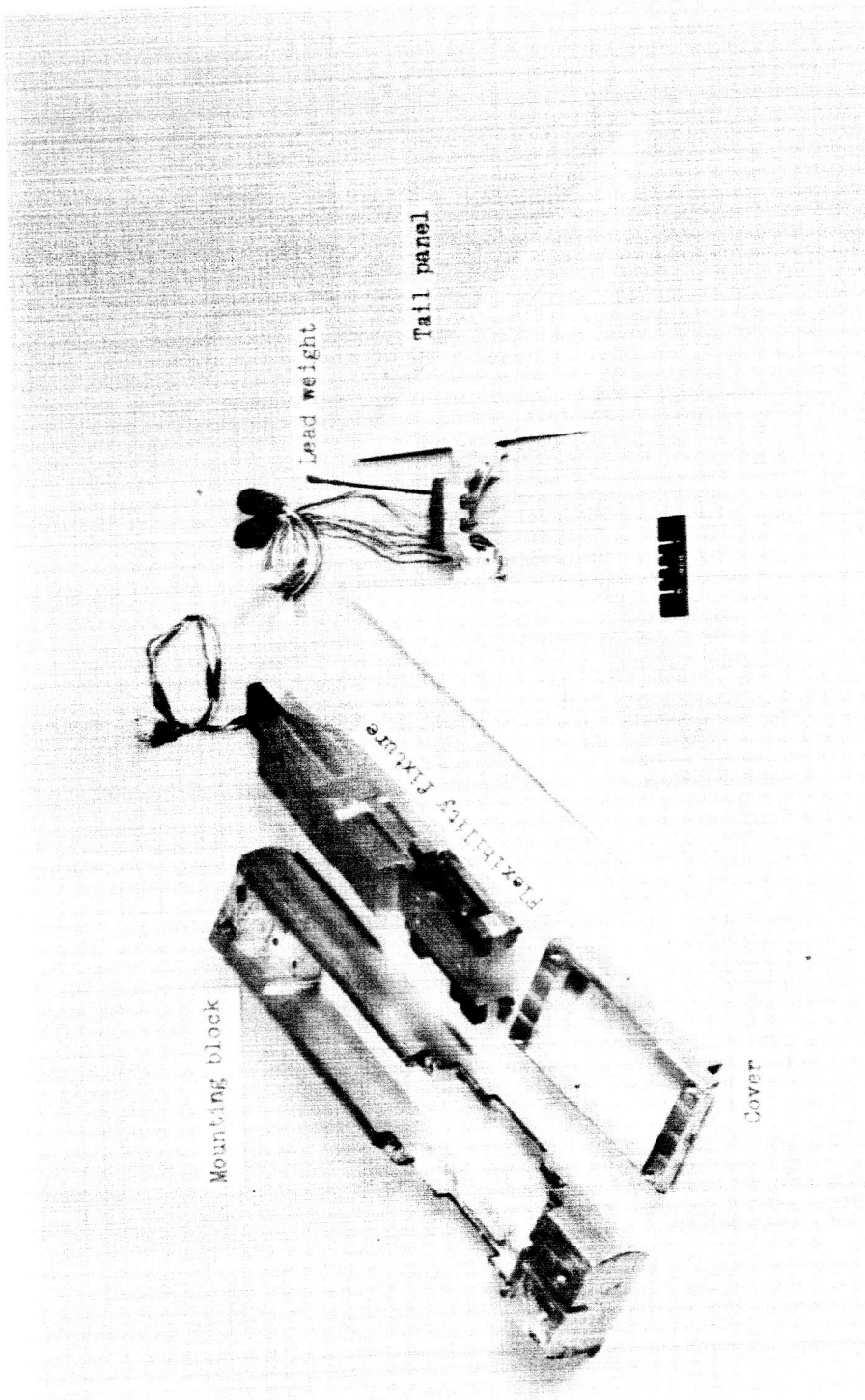

Figure 2.- Partially assembled model. L-57-386.1

Figure 3.- Assembled model. L-57-385

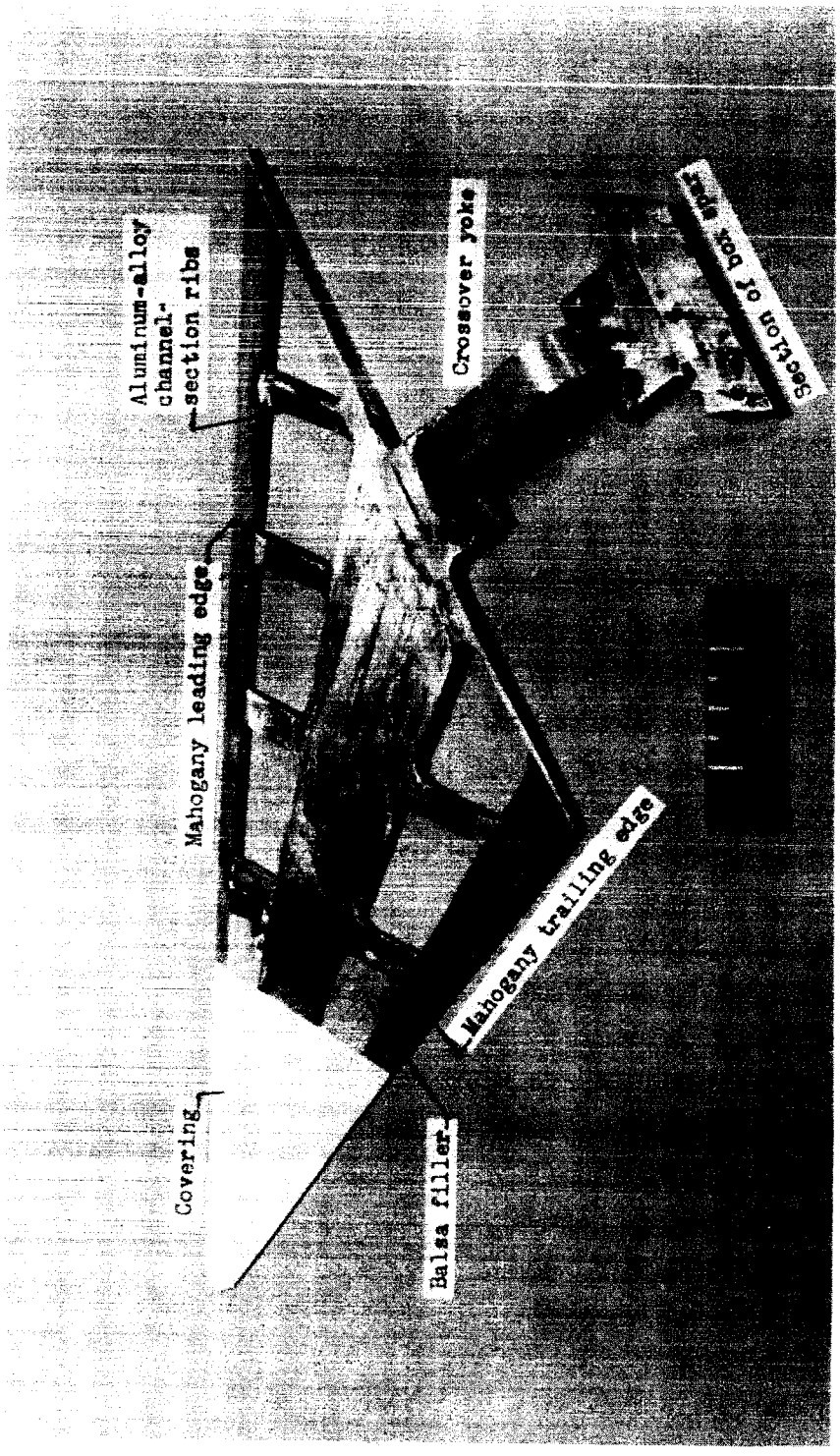

Figure 4.- Dissected panel showing method of construction. L-57-384.1

Figure 5.- Fuselage flexibility fixture. L-57-383.1

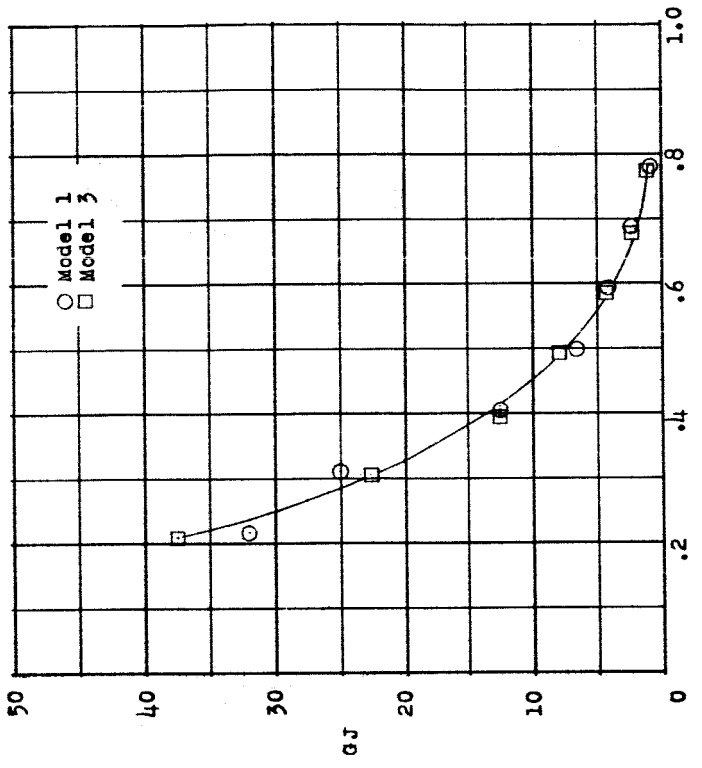

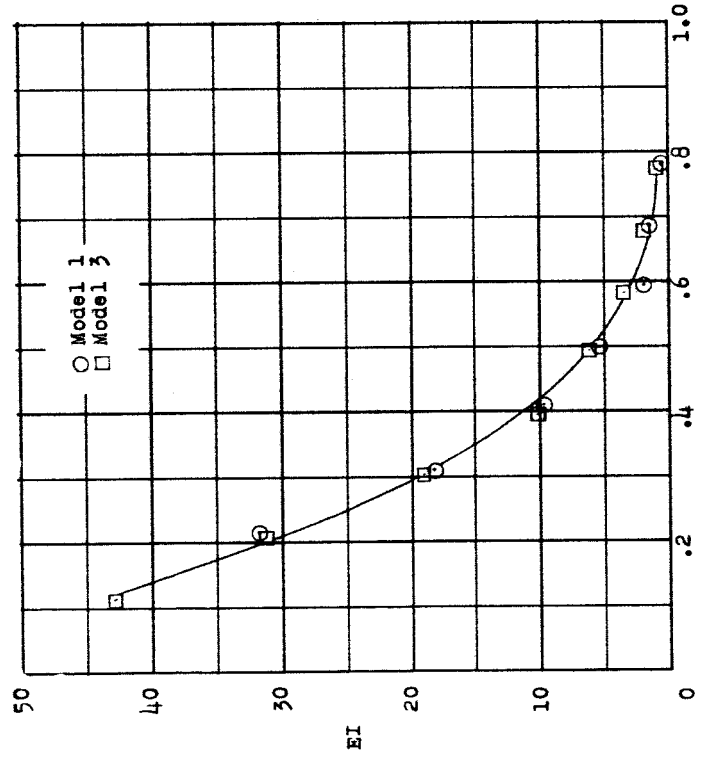

Figure 6.- Bending and torsional stiffnesses of models tested.

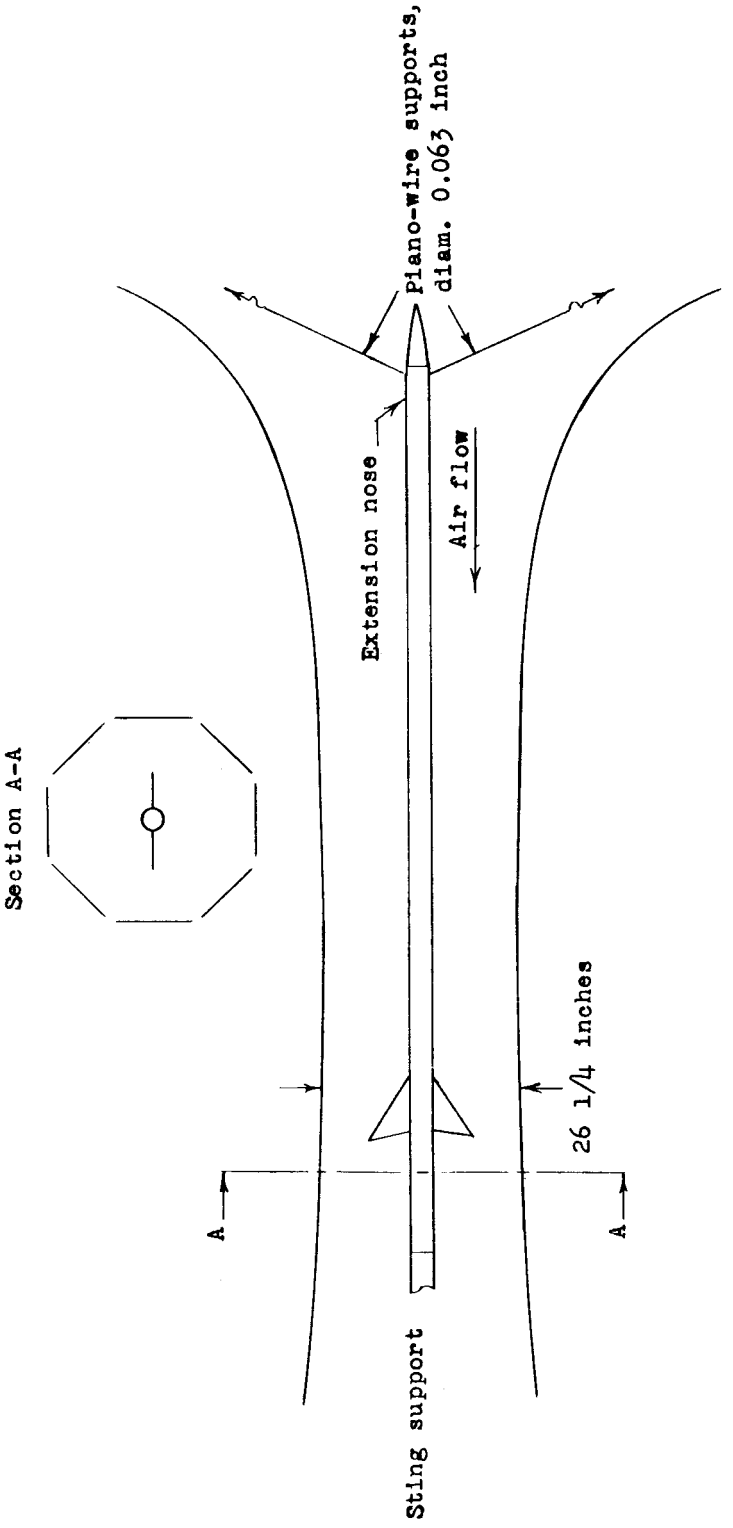

Figure 7.- Plan view of Langley transonic blowdown tunnel with flutter model installed.

Mode	Model			
	1		3	
	Left	Right	Left	Right
f_1	134	136	133	132
f_2	373	383	376	360
f_3	493	513	473	460
f_4	697	705	695	680
f_5	875	867	878	854

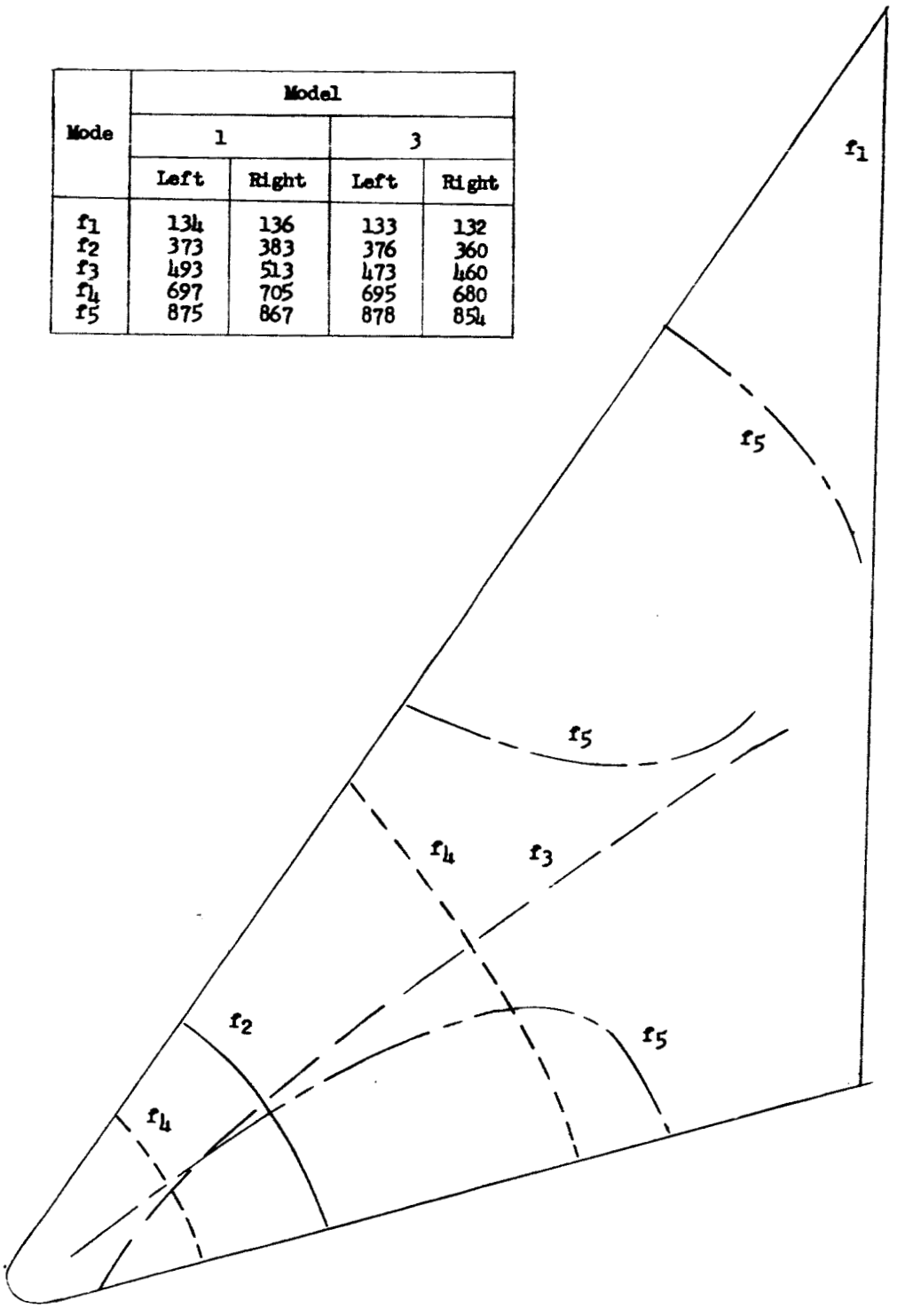

Figure 8.- Cantilever panel node lines and frequencies.

73 fuselage vertical bending
293 antisymmetrical yaw

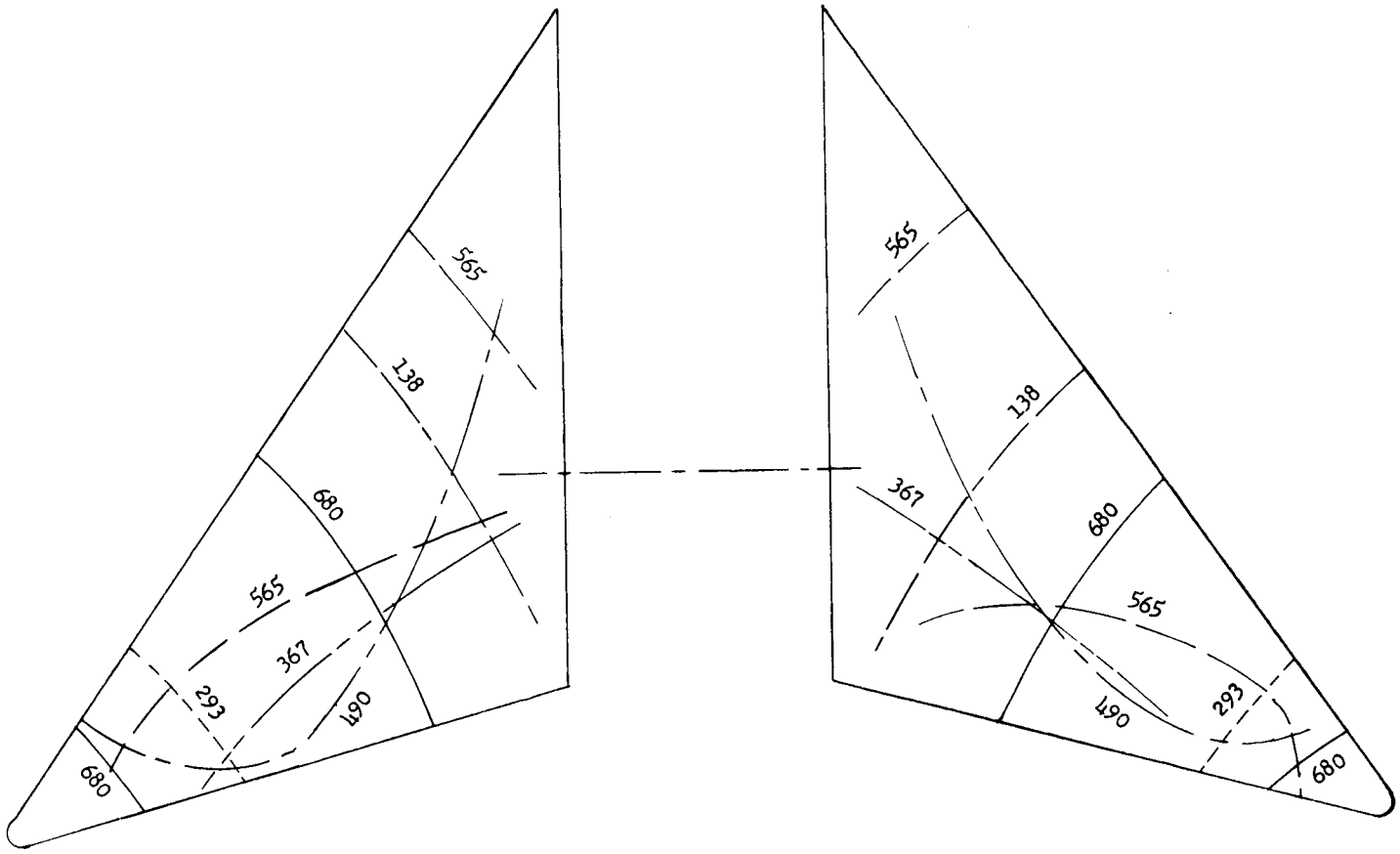

(a) Pitch axis rearward. Pitch stiffness, 788 ft-lb/radian.

Figure 9.- Node lines and frequencies with body freedoms. Frequencies in cycles per second.

70 fuselage vertical bending

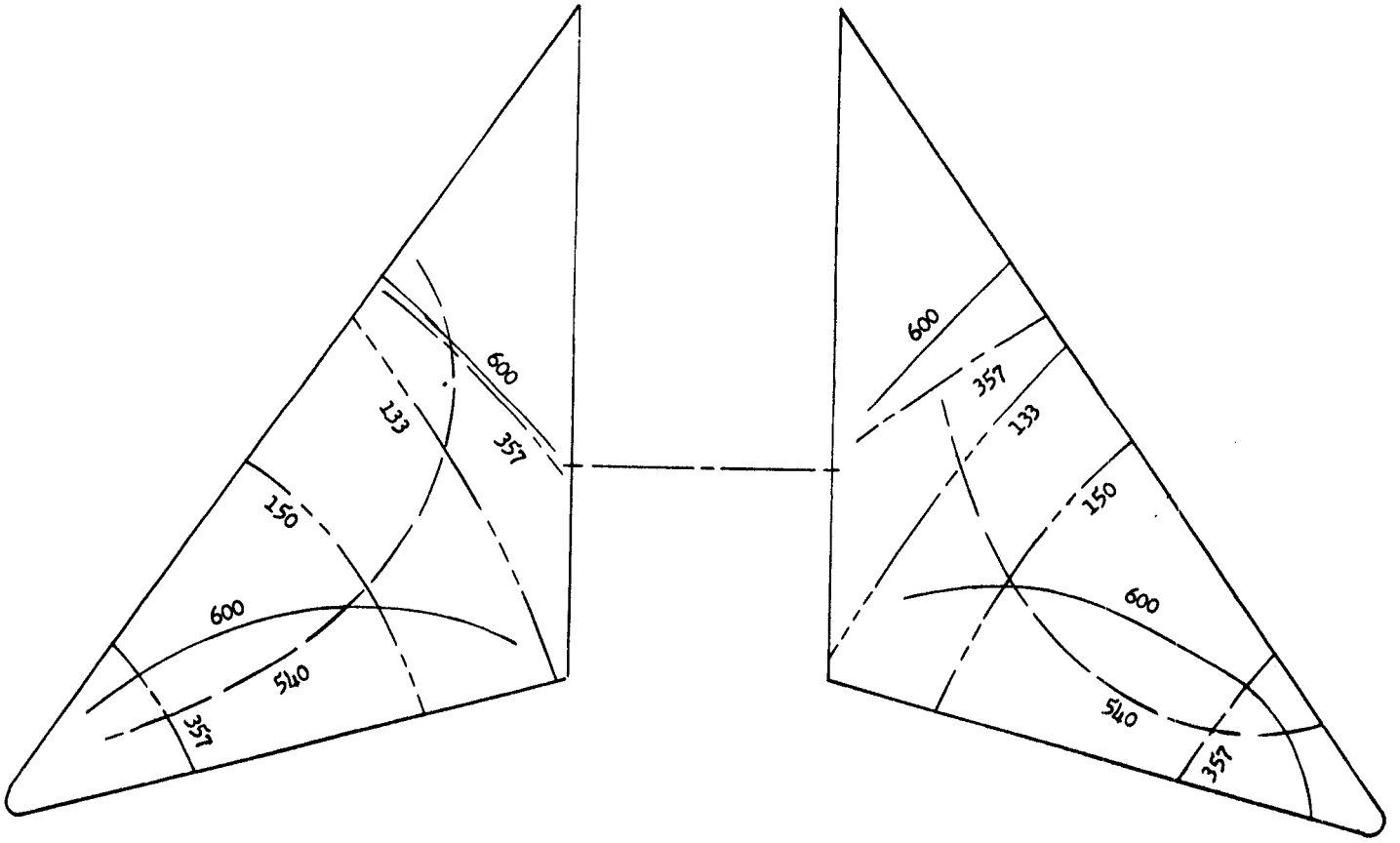

(b) Pitch axis rearward. Pitch stiffness, 1,093 ft-lb/radian.

Figure 9.- Continued.

73 fuselage vertical bending
93 fuselage roll
387, 390 symmetrical torsion
470 antisymmetrical torsion

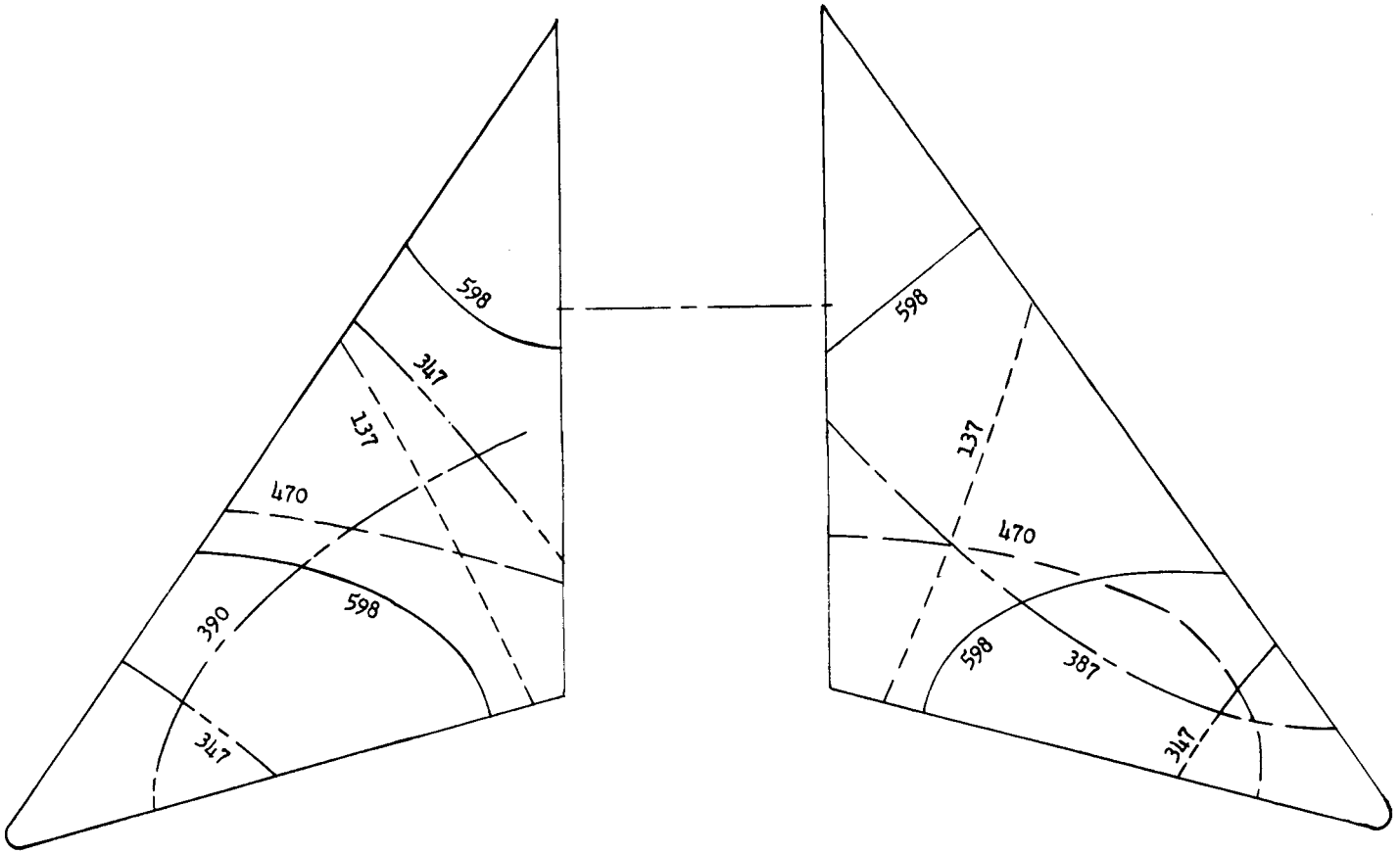

(c) Pitch axis forward. Pitch stiffness, 497 ft-lb/radian.

Figure 9.- Continued.

71.5 fuselage vertical bending
93.5 fuselage roll
200 antisymmetrical yaw
400 symmetrical torsion
473 antisymmetrical torsion

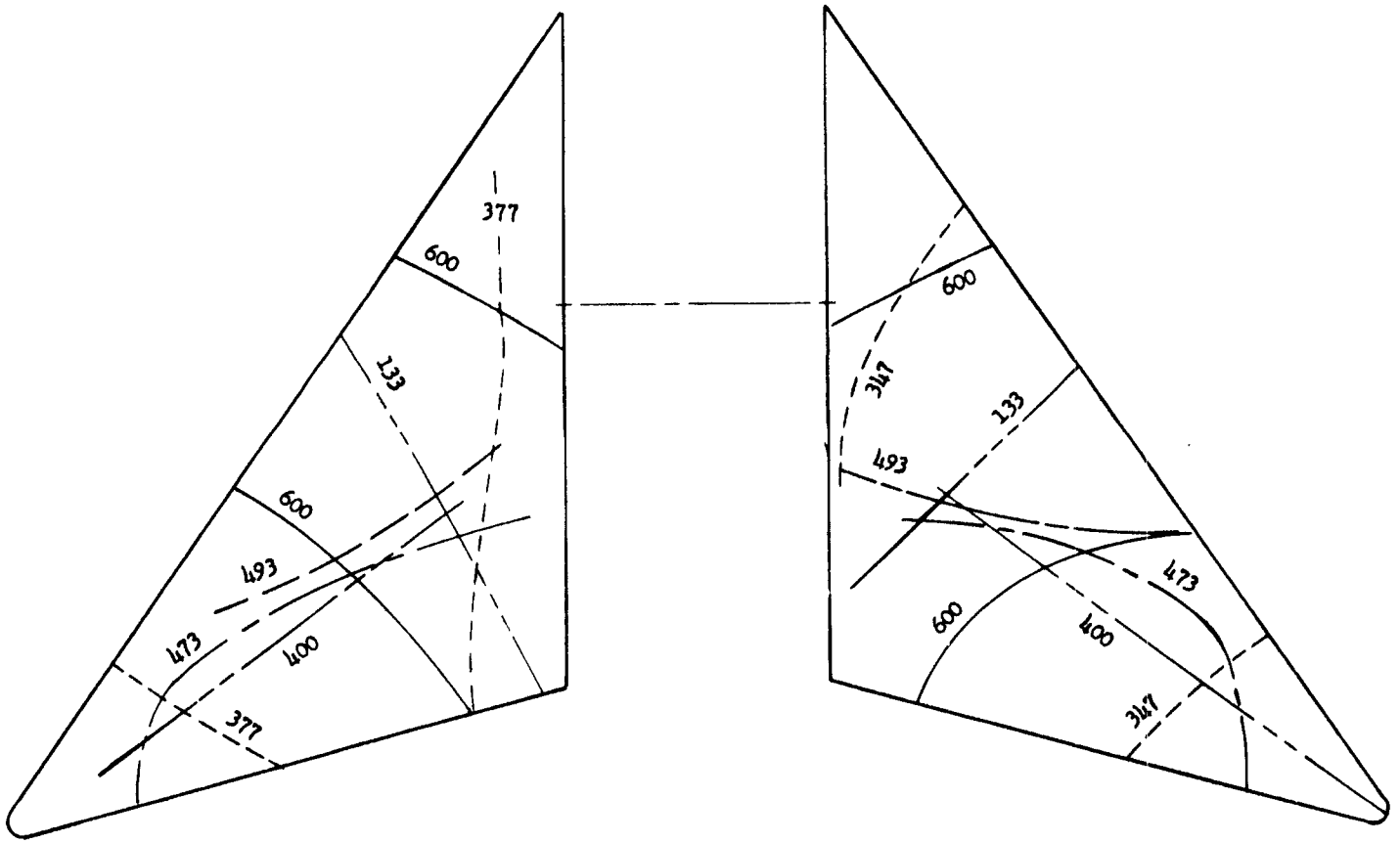

(d) Pitch axis forward. Pitch stiffness, 631 ft-lb/radian.

Figure 9.- Continued.

65 fuselage vertical bending
93 fuselage roll
245 antisymmetrical yaw

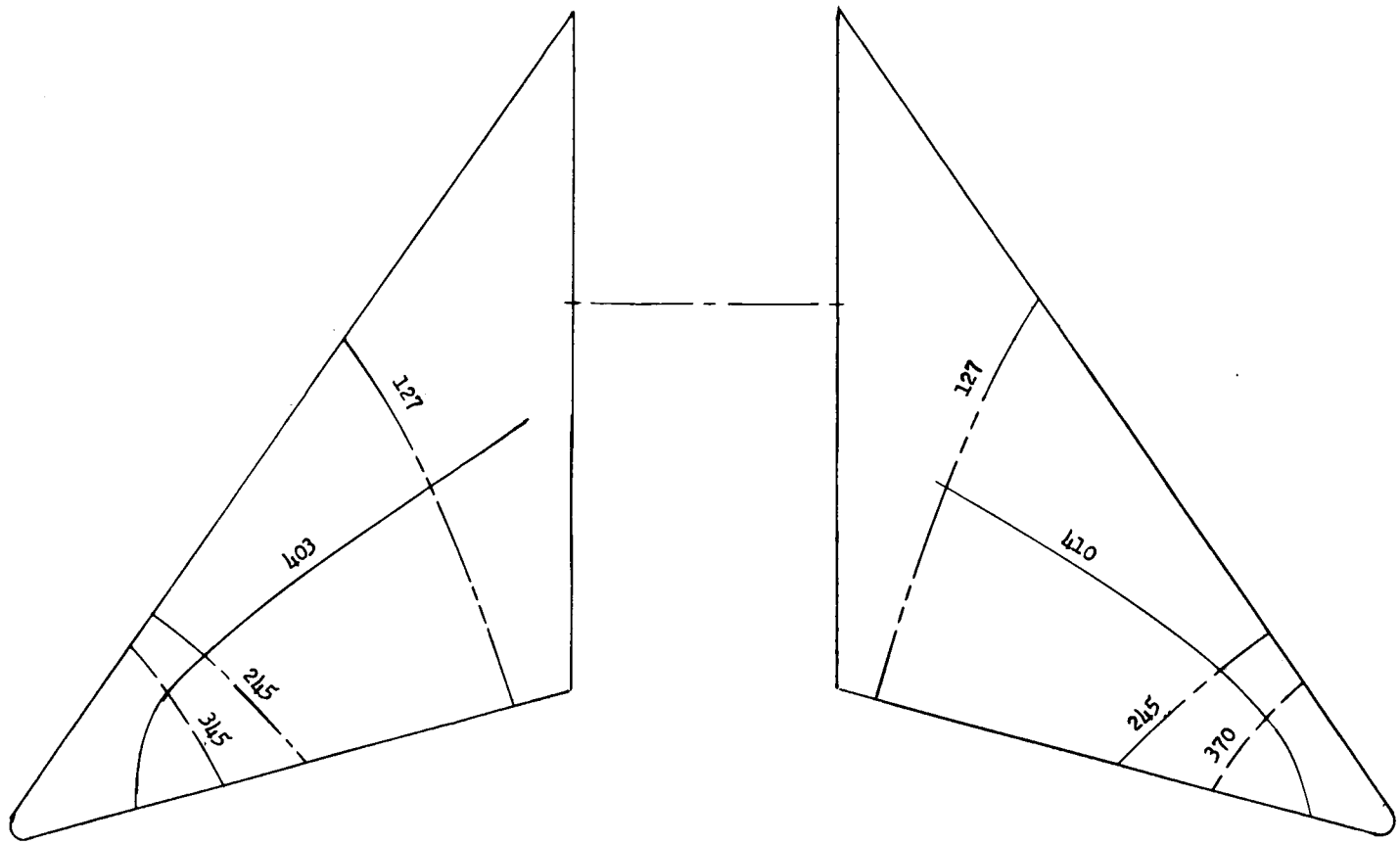

(e) Pitch axis forward. Pitch stiffness, 865 ft-lb/radian.

Figure 9.- Concluded.

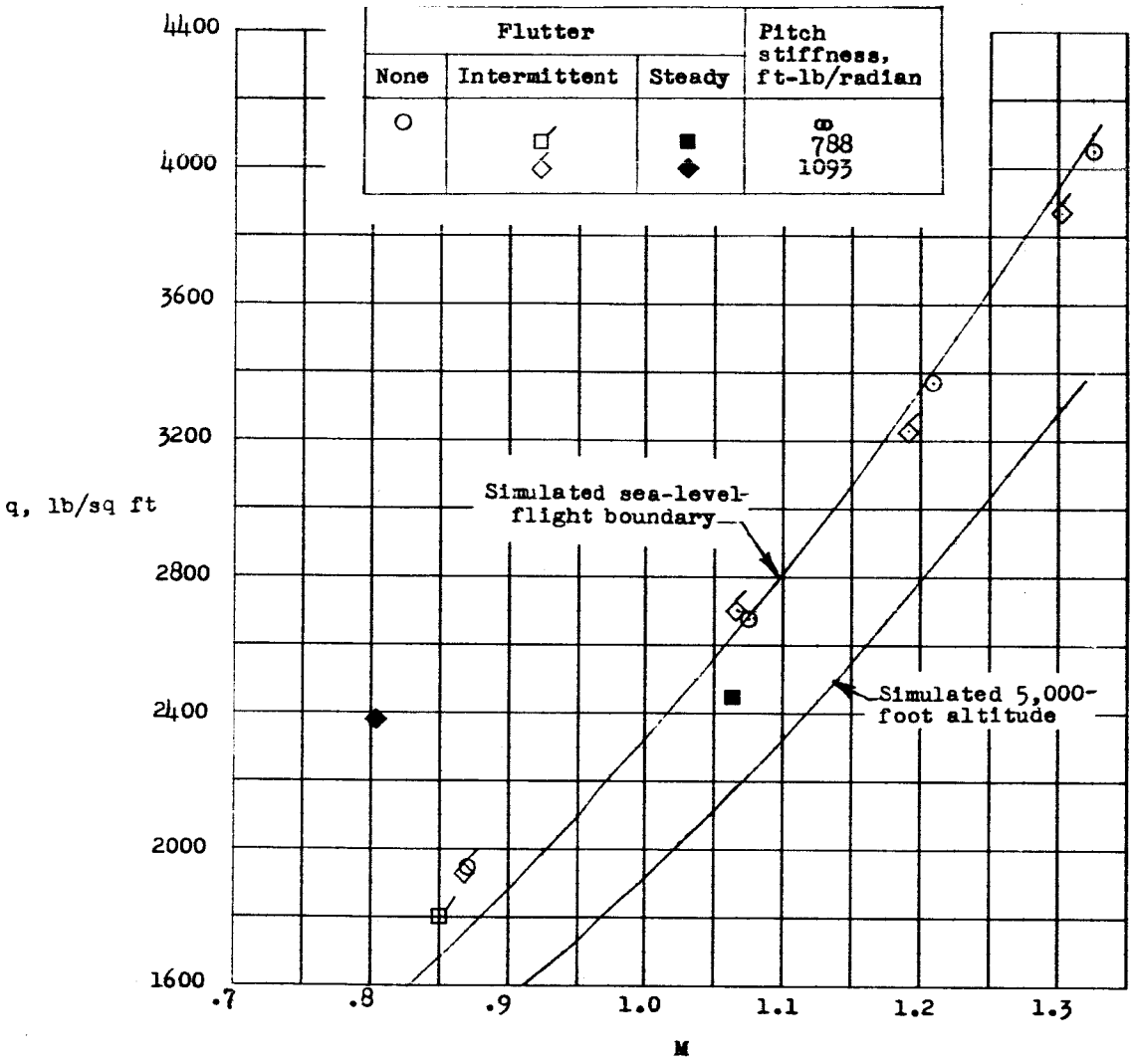

(a) Rearward pitch axis.

Figure 10.- Flutter data.

[redacted]

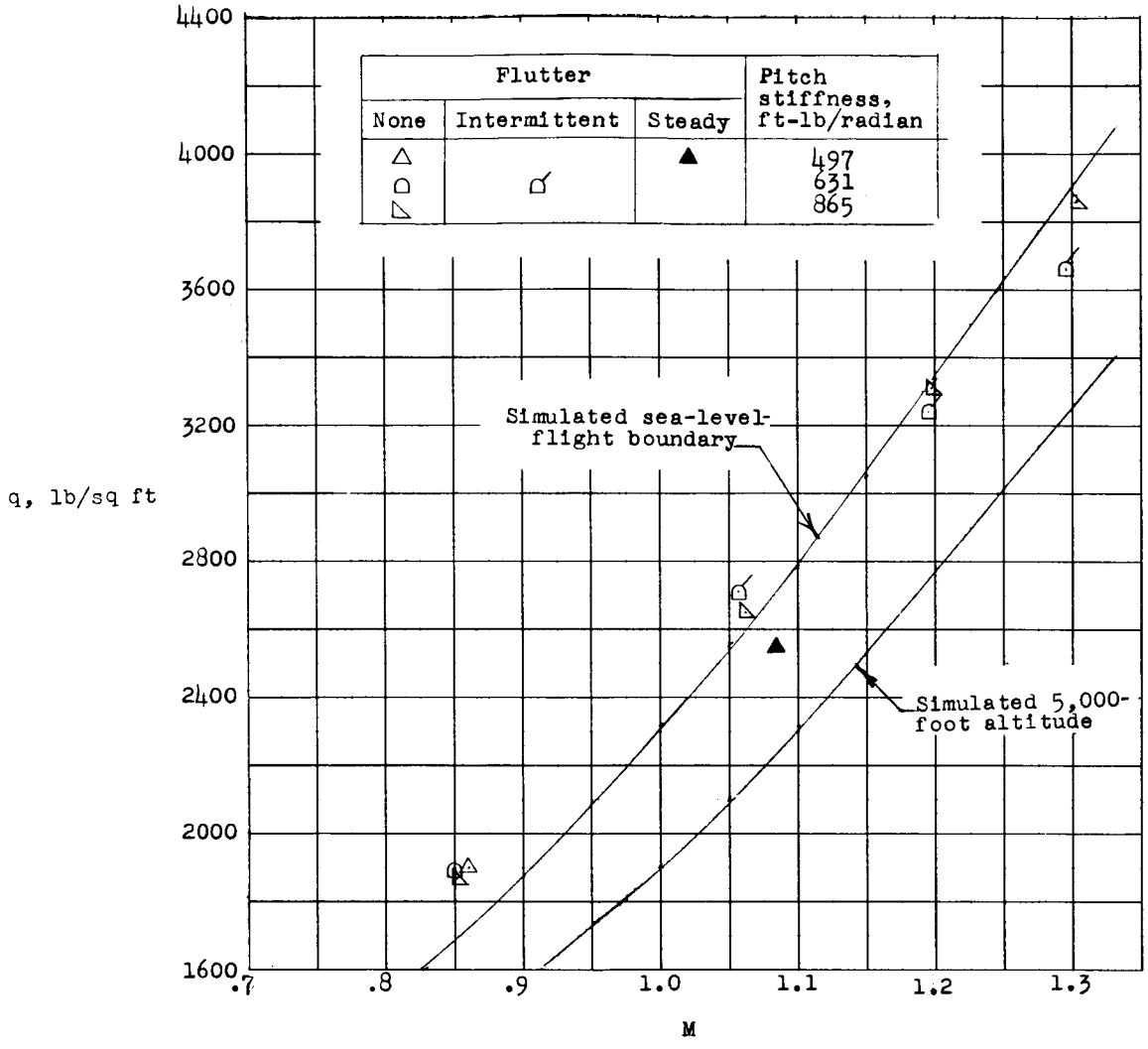

(b) Forward pitch axis.

Figure 10.- Concluded.